H-Atom Product Channels in the Photodissociation of CH_3Cl, CH_3Br, and CH_3I at 121.6 nm

Gabriel Amaral, Kesheng Xu, and Jingsong Zhang*

Department of Chemistry, University of California, Riverside, California 92521

Received: August 7, 2000; In Final Form: November 1, 2000

H-atom product channels in the photodissociation of jet-cooled methyl halides (CH_3X, X = Cl, Br, and I) at 121.6 nm are studied by using the high-*n* Rydberg-atom time-of-flight technique. Bimodal product center-of-mass (c.m.) translational energy distributions (with a fast and a slow component) and isotropic angular distributions have been observed. In going from CH_3Cl to CH_3Br to CH_3I, the translational energy of the fast component in the bimodal profiles decreases slightly, while that of the slow component, as well as its relative intensity, increases. The fast component, with a significant energy release, corresponds to direct production of $H + CH_2X(\tilde{X}^2B_1)$. The slow component, as suggested by the correlation of its translational energy distribution with the parent molecule CH_3X, might be mainly due to $H + H_2 + CX(X^2\Pi)$ and/or $X(^2P_{3/2})/X^*(^2P_{1/2}) + H + CH_2(X^3B_1)$ channels via the concerted three-body and/or two-step sequential dissociation. Although CH_3I is excited above its first two ionization thresholds, its neutral fragmentation could compete with the photoionization processes.

Introduction

Vacuum ultraviolet (VUV) photodissociation of methane and halogenated methanes has recently attracted considerable attention in the scientific community.[1−13] The most intense stream of work has focused on photodissociation of CH_4 via the $1t_2 \rightarrow 3s$ Rydberg transition at Lyman-α radiation (121.6 nm). The basics of this photodissociation have been elucidated by Mordaunt et al.,[1] and a number of recent papers have completed the picture.[2−7] A fast H-atom product channel (or two channels) that corresponds to $H + CH_3$ fragments was shown to be an important channel, and in addition, a slow H-atom channel was also observed, which is due to either sequential decomposition of the highly internally excited CH_3 fragment or concerted three-body fragmentation processes.[1−6] For photodissociation of methyl halides (CH_3X, X = Cl, Br, I), Tonokura et al. investigated the H-atom product channels at 157 nm using the resonance-enhanced multiphoton ionization (REMPI) technique and Doppler spectroscopy.[8] Brownsword et al. studied the H-atom channel in the photodissociation of CH_3Cl at 121.6 nm using H-atom laser-induced fluorescence (LIF).[9] Both studies observed similarly a Gaussian and a non-Gaussian component in the Doppler profiles of H-atom REMPI or LIF spectra and thus bimodal profiles in the product translational energy releases, which suggests two competitive mechanisms: (i) a direct C−H scission (the fast H-atom channel), corresponding to the $H + CH_2X$ products; and (ii) a two-step dissociation (the slow H-atom channel), via either a sequential decomposition of the highly internally excited CH_3 or CH_2X fragment, or dissociation via a highly excited CH_3X^{**} intermediate.[8,9] In the case of CH_3Cl, the total H-atom quantum yield increases from 0.29 at 157 nm to 0.53 at 121.6 nm, while the branching ratio of the fast/slow components decreases from 4 to 0.71.[8,9] For the fast component in the photodissociation of CH_3Cl at 121.6 nm, the average product translational energy $\langle E_T \rangle_{fast} = 0.57E_{avail}$, and for the slow component, $\langle E_T \rangle_{slow} = 0.10E_{avail}$.[9] For CH_3I photodissociation in the range of 140−170 nm, the C−H scission was shown to be the primary dissociation channel by Levy and Simons.[10] Photodissociation of related molecules such as CHF_2Cl at 121.6 nm has also been the subject of recent studies,[11,12] and similar bimodal (or even three-channel) profiles in the product translational energy release have been observed.

The similar behavior observed in the VUV photodissociation of CH_3Cl, CH_3Br, and CH_3I can be rationalized in terms of the corresponding electronic excitations. In all cases, a lone-pair $p\pi$ electron on the halogen atom is promoted to a molecular Rydberg state[13−20] that then undergoes dissociation. As the Rydberg excitation involves the nonbonding electron on the halogen atom, the excited state maintains a tetrahedral geometry similar to that of the ground state, and in addition, these Rydberg electronic transitions in methyl halides are very similar, with the only difference being the energy gaps between the electronic states.[13−20] At 121.6 nm, the electronic transition of CH_3Cl is $3p\pi \rightarrow 5p$ and/or 4d [i.e., the $(3e)^4 \rightarrow (3e)^3 5p$ or $(3e)^3 4d$ transitions, converging to the $^2E_{3/2}$ ion state at the first ionization threshold],[13−16] and that of CH_3Br is $4p\pi \rightarrow 9p$ (converging to the $^2E_{3/2}$ ion) or 7p′ (converging to the $^2E_{1/2}$ ion at the second ionization limit).[13,17,18] As Rydberg transitions decrease in energy in the order of $CH_3Cl-CH_3Br-CH_3I$, 121.6 nm radiation is slightly above the second ionization limit of CH_3I; the possible Rydberg transition of CH_3I at 121.6 nm is $5p\pi \rightarrow 13d'$ ($v_2' = 1$) (converging to the vibrationally excited $^2E_{1/2}$ ion state).[13,19,20] In the high-energy range above 78 000 cm^{-1} ($\lambda < 128$ nm), besides the structured sharp Rydberg absorption features, there is also an underlying broad background, which could be due to $\sigma \rightarrow \sigma^*$(C−X) and/or $\sigma \rightarrow \sigma^*$(C−H) valence transitions of methyl halides.[13−20] It is also worth noting that the main difference between the electronic excitation of methane and methyl halides is the lack of lone-pair electrons in methane, and thus higher Rydberg orbitals are involved in methyl halides at the same VUV excitation energy.

* Corresponding author. E-mail: jszhang@ucrac1.ucr.edu. Also at Air Pollution Research Center, University of California, Riverside, CA 92521.

10.1021/jp0028507 CCC: $20.00
Published on Web 01/30/2001

Despite a wealth of information available at the longer wavelengths in the UV region, much less is known about the photodissociation of methyl halides in the VUV region such as 121.6 nm. Specifically, no product angular distribution of CH_3Cl at 121.6 nm was previously measured, and the H-atom channels of CH_3Br and CH_3I at 121.6 nm have not been investigated before. In the present study, H-atom product channels in the photodissociation of CH_3Cl, CH_3Br, and CH_3I at 121.6 nm are studied. Product center-of-mass (c.m.) translational energy and angular distributions are obtained, which, along with their change and correlation with the parent molecules, reveal detailed information about the VUV photodissociation dynamics (particularly the decay of high Rydberg states) of CH_3X.

Experimental Section

H-atom product time-of-flight (TOF) spectra were obtained by using the high-*n* Rydberg atom TOF technique that has been described previously.[21,22] A pulsed molecular beam was produced by expanding a mixture of ~5% CH_3Cl, CH_3Br, or CH_3I in He carrier gas at a total pressure of 100 kPa into the source chamber through a pulsed nozzle. The pulsed beam was collimated by a 1 mm diameter skimmer 2.8 cm from the nozzle. At 4.6 cm further downstream in the main chamber, the beam was crossed with the VUV radiation tuned to the Lyman-α transition at 121.6 nm. This VUV radiation was generated by tripling the 364.7 nm UV radiation [doubled output from a Nd:YAG pumped dye laser (Lambda-Physik 3002)] in Kr, and was focused into the interaction region by a MgF_2 lens, and its polarization could be changed by rotating the polarization of the 364.7 nm UV light with a $\lambda/2$ plate.[6] The 121.6 nm radiation first induced photodissociation of the methyl halide molecules. The H atoms produced were subsequently excited to the 2^2P electronic state by the same 121.6 nm radiation. These H atoms were further excited from the 2^2P level to a high-*n* Rydberg level ($n \sim 40-90$) by the doubled output (~366 nm) from another Nd:YAG pumped dye laser (Laser Analytical System 2051). Background ions (generated by photolysis or probe laser beams) were removed by a small negative potential applied below the interaction region and thus were prevented from reaching the detector. The high-*n* Rydberg H-atom fragments are radiatively metastable and drifted with their nascent velocities to a microsphere plate detector (El-Mul Technologies) with the TOF path perpendicular to both the molecular beam and the laser beams. Upon arrival at the detector, the excited atoms were field-ionized as they passed a wire mesh and were then detected as ions. The nominal flight distance was 37.1 cm. TOF spectra were recorded and averaged by using a multichannel scaler (EG&G, Turbo MCS, dwell time 20 ns), and the spectra shown in this work represent 100−200k laser firings. As the 364.7 nm UV radiation was not separated from the Lyman-α radiation and the 366 nm probe was slightly focused in the interaction region in our experimental setup, one need to consider possible signals due to multiphoton dissociation by the UV radiation, in addition to the weak signals from 121.6 nm photodissociation. However, our results for CH_3Cl (discussed below) were very similar to those by Brownsword et al. (in which the Lyman-α radiation was carefully separated from the 212.5 nm UV radiation and no 366 nm probe was used),[9] suggesting little or no contribution from the UV radiation. Furthermore, the fast H atoms (with $E_T > 55$ kcal/mol) observed in our TOF spectra (discussed below) were beyond the energetic limit of two-photon dissociation by the 365 nm radiation, and should be due to only the 121.6 nm photodissociation.

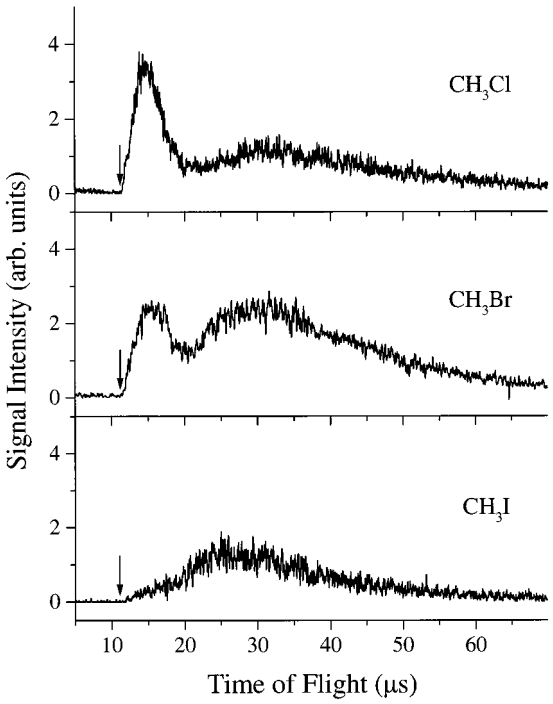

Figure 1. H-atom TOF spectra of photodissociation of CH_3Cl, CH_3Br, and CH_3I by 121.6 nm radiation (with its polarization parallel to the TOF axis). The spectra have been normalized to the same number of laser shots. The arrow indicates the threshold of the H + CH_2X channel (the lowest-energy H-atom product channel).

Results

Figure 1 shows the H-atom TOF spectra from photodissociation of CH_3Cl, CH_3Br, and CH_3I at 121.6 nm, with the polarization of the VUV radiation parallel ($\theta = 0°$) to the TOF axis. TOF spectra at perpendicular ($\perp$, $\theta = 90°$) polarization were also obtained, and they were identical to those at $\theta = 0°$. A separate experiment indicated that the detection sensitivity of H atoms was the same for both polarizations of the VUV radiation. Product c.m. translational energy distributions at the two polarization angles, $P(E_T,\theta)$'s, are derived from the TOF spectra,[21,22] and $P_{||}(E_T)$'s are shown in Figures 2−4. Depending on the dissociation channels and mechanisms, the counterfragment of the H atom can be different. However, due to the small mass of the H atom compared to other photofragments, the difference in E_T due to conversion of the TOF spectra to $P(E_T)$'s is insignificant. For convenience, CH_2X is chosen as the counterfragment for deriving $P(E_T)$'s, which is exact for the H + CH_2X channel (the fast component in the $P(E_T)$'s, discussed below).

The product c.m. translational energy and angular distribution for the photodissociation is expressed as[23] $P(E_T,\theta) = (1/4\pi)P(E_T)[1 + \beta(E_T)P_2(\cos\theta)]$, where β is the anisotropy parameter ($-1 \le \beta \le 2$), θ is the angle between the electric vector of the polarized VUV radiation and the recoiling velocity vector of the H-atom product (the direction of detection) in the c.m. frame, $P_2(\cos\theta)$ is the second Legendre polynomial, and $P(E_T)$ is the product c.m. translational energy distribution. β is calculated by using $\beta(E_T) = 2[P_{||}(E_T) - P_{\perp}(E_T)]/[P_{||}(E_T) + 2P_{\perp}(E_T)]$. The β parameters of CH_3Cl and CH_3Br are essentially zero (with some fluctuation due to noise) (Figures 2 and 3), and their product angular distributions are isotropic for both the fast and slow components. Thus, $P_{||}(E_T)$'s are independent of β and θ, and are equivalent to $P(E_T)$'s and used for calculation of translational energy release and product branching ratios (Figures 2−4).

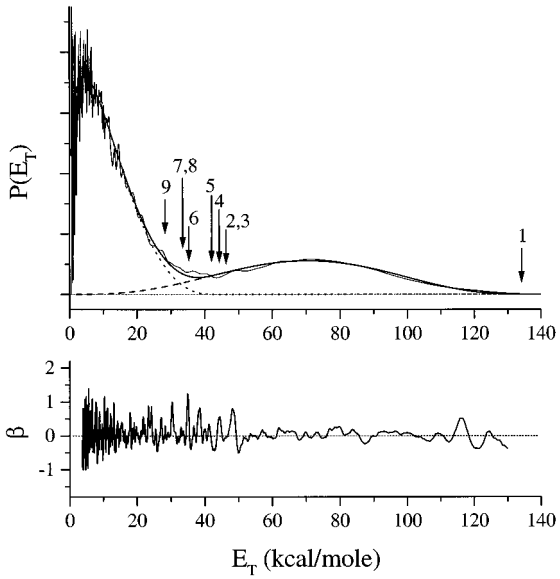

Figure 2. Upper: product c.m. translational energy distribution, $P(E_T)$, of the H-atom product channel in 121.6 nm photodissociation of CH_3Cl, converted from the TOF spectrum in Figure 1. The experimental $P(E_T)$ (in thin solid line) has been slightly smoothed by fast Fourier transformation. The overall fitting (in thick solid line) and the deconvoluted slow (in dot line) and fast (in dash line) components are plotted. The arrows indicate the thresholds for H-atom production channels 1−9. See text for more details. Lower: anisotropy parameter β of the H-atom product channels as a function of E_T.

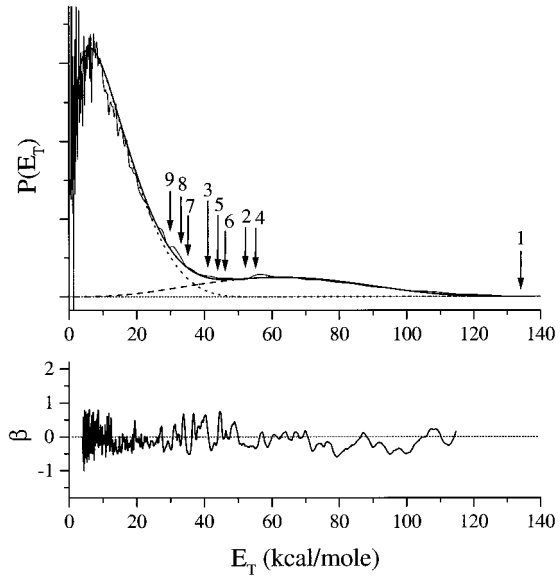

Figure 3. Same as in Figure 2, except for CH_3Br.

The most important feature in the $P(E_T)$'s is the bimodal profiles, in agreement with the 121.6 nm study of CH_3Cl by Brownsword et al.[9] and similar to the results for CH_3Cl, CH_3Br, and CH_3I at 157 nm by Tonokura et al.[8] The bimodal profiles suggest at least two different mechanisms for the formation of H-atom fragments. Similar to the studies by Tonokura et al.[8] and Brownsword et al.,[9] the $P(E_T)$'s of the three methyl halides are deconvoluted by fitting with two peaks. An RRK-type functional form, $P(E_T) = A(E_T)^p(E_0 - E_T)^q$, is utilized, with A, p, and q as the adjustable parameters. E_0 corresponds to the maximum available energy of each component. For the fast peak, E_0 is chosen to be fixed at E_{avail} (134 kcal/mol), while for the slow peak, it is adjustable. This functional form provides good fits to both the fast and the slow peaks, and the deconvolution results are shown in Figures 2−4. The deconvoluted $P(E_T)$'s for the fast and slow components are similar to those obtained by Brownsword et al.[9] Furthermore, the relative branching ratio of the fast and slow components decreases from CH_3Cl, CH_3Br, to CH_3I, similar to 157 nm photodissociation by Tonokura et al.[8] The properties of the bimodal profiles, such as the translational energy release and branching ratios, are summarized in Table 2.

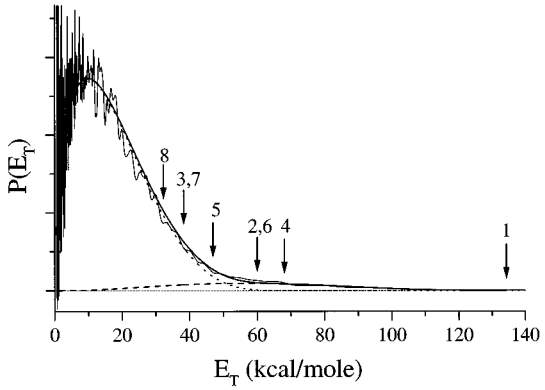

Figure 4. Same as in Figure 2, except for the $P(E_T)$ of CH_3I only.

Discussion

1. Possible H-Atom Production Channels and the Electronic Transitions. Upon the 121.6 nm excitation, there are nine energetically possible, spin-allowed H-atom product channels of the CH_3X molecules. These channels are listed in the order of increasing enthalpy of reaction, $\Delta H_r°$, for CH_3Cl:

$$CH_3X(\tilde{X}\,^1A_1)\ (+h\nu) \longrightarrow H(^2S) + CH_2X(\tilde{X}\,^2B_1) \quad (1)$$

$$H_2(X^1\Sigma_g^+) + CHX(\tilde{X}\,^1A') \quad (2)$$

$$\hookrightarrow H + CX(X^2\Pi)$$

$$HX(X^1\Sigma^+) + CH_2(\tilde{a}\,^1A_1) \quad (3)$$

$$\hookrightarrow H + CH(X^2\Pi)$$

$$X(^2P_{3/2}) + CH_3(\tilde{X}\,^2A_2'') \quad (4)$$

$$\hookrightarrow H + CH_2(\tilde{X}\,^3B_1)$$

$$X(^2P_{1/2}) + CH_3(\tilde{X}\,^2A_2'') \quad (5)$$

$$\hookrightarrow H + CH_2(\tilde{X}\,^3B_1)$$

$$X(^2P_{3/2}) + CH_3(\tilde{X}\,^2A_2'') \quad (6)$$

$$\hookrightarrow H + CH_2(\tilde{a}\,^1A_1)$$

$$X(^2P_{1/2}) + CH_3(\tilde{X}\,^2A_2'') \quad (7)$$

$$\hookrightarrow H + CH_2(\tilde{a}\,^1A_1)$$

$$H(^2S) + CH_2X(\tilde{X}\,^2B_1)$$

$$\hookrightarrow H + CHX(\tilde{X}\,^1A') \quad (8)$$

$$\hookrightarrow H + CHX(\tilde{a}\,^3A'') \quad (9)$$

As limited spectroscopic and thermodynamic information is available for the CH_2X, CHX and CX species (X = Cl, Br, I), the energy thresholds of the various dissociation channels are estimated with considerable uncertainties. Table 1 lists the values of $\Delta H_r°$ (calculated from literature heats of formation and electronic and spin−orbit splitting energies[24−30]) for the nine

TABLE 1: Enthalpy of Reactions ΔH_r° (kcal/mol) for the Nine Possible H-Atom Production Channels[a]

channel	CH_3Cl	CH_3Br	CH_3I
(1)	101 ± 2	101 ± 2	101 ± 1
(2)	189 ± 5	183 ± 15	175
(3)	189 ± 4	194 ± 4	197 ± 4
(4)	191 ± 1	180 ± 2	167 ± 2
(5)	193 ± 1	191 ± 2	188 ± 2
(6)	200 ± 1	189 ± 2	176 ± 2
(7)	202 ± 1	200 ± 2	197 ± 2
(8)	201 ± 5	202 ± 5	203 ± 5
(9)	207 ± 5	205 ± 5	

[a] The ΔH_r° values are referred to the final products (i.e., triple fragments for channels 2−9) and are calculated without including the 121.6 nm photon energy. Due to the large uncertainties in the thermodynamical values of the methyl halide systems, corrections of enthalpies of reaction from 298 to 0 K are generally within the error limits. Literature values (including electronic energies) are from refs 24−30.

H-atom product channels of CH_3Cl, CH_3Br, and CH_3I. The expected onsets of these product channels in CH_3Cl, CH_3Br, and CH_3I are also labeled in the $P(E_T)$'s in Figures 2−4. Channel 1 is the only two-fragment H-atom product channel. Others [(2)−(9)] involve three fragments (including at least one H atom) via either sequential two-step (as described in eqs 2−9 and only spin-allowed first steps are considered) or concerted three-body dissociation processes, although the three final fragments are not distinguishable in both cases.

The electronically excited states upon 121.6 nm excitation in all the three CH_3X are predominantly due to Rydberg transitions, resulting from promotion of a p electron on the halogen to a higher p or d Rydberg orbital (i.e., an e → e promotion in the C_{3v} molecule), while the $\sigma \rightarrow \sigma^*$ valence transition might also be involved.[13−20] Since the Rydberg electron interacts with the ionic core ($^2E_{3/2}$ and $^2E_{1/2}$), the resulting excited state could in principle exhibit either A_1, A_2, or E character in the C_{3v} point group.[13,16,20] However, as the $A_1 \rightarrow A_2$ transition is forbidden, the ground-state $CH_3X(\tilde{X}^1A_1)$ can be excited only to a A_1 or E excited states via the one-photon VUV photoexcitation. For the high Rydberg states to dissociate into the low-lying neutral fragments, the initial electronic energy of the Rydberg electron has to be transferred to the nuclei or the molecular ion core (accompanied with exchange of angular momentum),[31−33] which in general could be facilitated by nonadiabatic processes such as crossings of the Rydberg states with the low-lying (repulsive) valence states or the repulsive walls of the bond valence states. As the Rydberg electron spends most of the time away from the ionic core, the strength of the Rydberg−valence interactions and thus the radiationless transition rate is $\propto n^3$ (i.e., the probability for penetrating to the ionic core), where n is the principle quantum number of the Rydberg state.[16,31−33] Also, the strength of the interactions scales with s > p(π) > d, in the order of decreasing overlap of the Rydberg orbital and the molecular frame.[13,16] Finally, multiple steps of couplings may be required in the radiationless decay and dissociation of the high Rydberg states.[34]

2. The Fast Component in the $P(E_T)$'s. The fast component in the $P(E_T)$'s (i.e., the narrow peak at early time in the TOF spectra) corresponds to the $H + CH_2X(\tilde{X}^2B_1)$ channel 1, since this is the only possible H-atom dissociation channel in the high E_T region (Figures 2−4). In the dissociation of CH_3X (in C_{3v}) into $H + CH_2X(\tilde{X}^2B_1)$ [in C_{2v}, with the unpaired carbon p electron perpendicular to the plane (yz) of the radical], the conserved symmetry element is the reflection plane (xz) that bisects the HCH group of CH_3X and perpendicular to the yz molecular plane of CH_2X. If the H atom leaves in the xz plane (the plane of reflection) and thus a C_s symmetry is assumed for the dissociation process, the ground-state $CH_2X(\tilde{X}^2B_1)$ (reduced to $^2A'$ in C_s) product correlates adiabatically with the ground-state $CH_3X(^1A_1)$ (reduced to $^1A'$) and the $1^3A'$ state (in C_s). On the other hand, the highly excited Rydberg states of CH_3X accessed by the VUV photoexcitation, which are of A_1 and E characters in the C_{3v} geometry and are reduced to A′ and A′ + A″ in C_s, correlate with higher electronic states (including Rydberg levels) of the $CH_2X + H$ fragments.[5] Therefore, nonadiabatic processes such as internal conversion (IC) to the ground-state $CH_3X(^1A')$ and/or intersystem crossing (ISC) to the low-lying $1^3A'$ state are required for the higher Rydberg states of CH_3X to dissociate into the $H + CH_2X(\tilde{X}^2B_1)$ products. Similarly, in the VUV photodissociation of CH_4 via the $1t_2 \rightarrow 3s$ excitation, dissociation mechanisms by IC to the $1^1A'$ ground state and ISC to the $1^3A'$ state have been proposed for the $H + CH_3(\tilde{X}^2A_2'')$ channels.[1,5,6]

The average translational energy release of the fast peak is 0.52, 0.47, and 0.44 of E_{avail} in CH_3Cl, CH_3Br, and CH_3I, respectively. This $\langle E_T \rangle$ is significantly larger and more repulsive than that in a statistical dissociation, suggesting a primary and nonstatistical dissociation process. Similarly, the fast component of the $H + CH_3(\tilde{X}^2A_2'')$ product channels in the 121.6 nm photodissociation of CH_4 has a comparable translational energy release, and is believed to be produced from dissociation on the repulsive (along the C−H coordinate) triplet $1^3A'$ surface of CH_4 after ISC from the 3s Rydberg level.[5,6] If the same mechanism is true for CH_3X, the fast component should be more likely due to final dissociation from the $1^3A'$ state, instead of from the $1^1A'$ ground state, after crossing from the higher Rydberg states. It should be pointed out that in the photodissociation of CH_3Cl at 193 nm, the translational energy release of the $H + CH_2Cl$ channel (a minor channel with an H-atom quantum yield of 0.01) is $0.44E_{avail}$,[36] where only the valence transition $\sigma \rightarrow \sigma^*$(C−Cl) [with small mixing with $\sigma \rightarrow \sigma^*$(C−H)], rather than the Rydberg transition, is involved.[13] The broad underlying absorption features of CH_3X due to the $\sigma-\sigma^*$ excitation at the high-energy region ($\lambda < 128$ nm)[13] may also contribute to the $H + CH_2X$ dissociation channel, as well as the $CH_3 + X$ channel (which could then undergo secondary decomposition to produce slow H atoms).

As the transition dipole moment of the $A_1 \rightarrow A_1$ transition is along the C−X axis (z), if the H atom dissociates from the A_1 state in its initial configuration (i.e., in a prompt dissociation), the anisotropy parameter β, based on the H−C−X angle,[27] is

TABLE 2: Properties of the Fast and Slow Components in the Bimodal $P(E_T)$'s of 121.6 nm Photodissociation of CH_3X

	E_{avail} (kcal/mol)	$\langle f_T \rangle_{slow}$[a]	$(E_T^{peak})_{slow}$[b] (kcal/mol)	$\langle f_T \rangle_{fast}$[a]	$(E_T^{peak})_{fast}$[b] (kcal/mol)	I_{fast}/I_{slow}[c]	ref
CH_3Cl	134	0.08	4	0.52	70	0.54	this work
		0.10		0.57		0.71 ± 0.15	ref 9
CH_3Br	134	0.10	6	0.47	62	0.24	this work
CH_3I	134	0.13	10	0.44	56	0.08	this work

[a] $\langle f_T \rangle = \langle E_T \rangle / E_{avail}$. [b] E_T^{peak} is the peak translational energy of each component. [c] Branching ratio based on the integrated areas of the fast and slow components.

estimated to −0.64.[8] On the other hand, the transition moment of $A_1 \rightarrow E$ lies in the plane (*xy*) perpendicular to the C−X axis, and a β parameter of 0.33 is predicted for a prompt photodissociation from the E state.[8] However, the experimental β parameter of the fast component, based on the studies of CH_3Cl and CH_3Br, is essentially zero, revealing an isotropic angular distribution. The $\beta \approx 0$ could be due to mixed and averaged contributions from both the A_1 and E excited states. This mechanism requires fast IC and ISC from the excited states of CH_3X and prompt subsequent dissociation into the $H + CH_2X(\tilde{X}^2B_1)$ products, as in the case of the fast $H + CH_3(\tilde{X}^2A_2'')$ photodissociation channels in CH_4 (which have anisotropic angular distributions).[6] However, the complex nonadiabatic couplings of the *n*p and *n*d high Rydberg states and the valence states might slow down the decay of CH_3X from the high Rydberg states to the ground state or the low-lying triplet state. Alternatively, the isotropic angular distribution could be due to a longer time scale of dissociation (in the order of a rotational period of the parent molecules).

3. The Slow Component in the $P(E_T)$'s. While the fast peak in the $P(E_T)$'s shifts to lower energy from CH_3Cl to CH_3Br to CH_3I, the slow peak broadens and shifts to higher energy, with $\langle f_T \rangle = 0.08$, 0.10, and 0.13, respectively (Figures 2−4 and Table 2). The slow $P(E_T)$ is essentially in a Maxwell−Boltzmann energy distribution (typical in a statistical dissociation process), and it also has an isotropic angular distribution. This slow component likely results from triple dissociation channels 2−9 (whose energy thresholds are indicated in Figures 2−4), via either concerted three-body or sequential two-body dissociation. Note that these slow H atoms must be produced within the 7 ns pulse of the VUV radiation. While the concerted three-body dissociation pathways in channels 2−9 should be allowed,[5a] some of the two-step sequential dissociation pathways in (2)−(9) could be restricted by symmetry and spin conservation. In channels 2 and 3, triplet CHX and CH_2 are not considered in the first step, while the singlet $CHX(\tilde{X}^1A')$ and $CH_2(\tilde{a}^1A_1)$ correlate with $H + CX(X^2\Pi)$ and $H + CH(X^2\Pi)$, respectively, in the A′ symmetry (assuming a planar dissociation), and thus can readily undergo unimolecular decomposition in the second step (provided that enough energy is available). The second step in channels 4−7 correspond to unimolecular dissociation of $CH_3(\tilde{X}^2A_2'')$ into an H atom and one of the two energetically possible states of CH_2. As the ground-state $CH_3(\tilde{X}^2A_2'')$ correlates adiabatically to $H + CH_2(\tilde{X}^3B_1)$ and the excited-state $CH_3(\tilde{B}^2A_1)$ to $H + CH_2(\tilde{a}^1A_1)$,[35] in the two-step dissociation pathways, channels 4 and 5 should be more important than (6) and (7). In channels 8 and 9, assuming a planar dissociation in the second step, $CH_2X(\tilde{X}^2B_1)$ (reduced to $^2A''$ in the C_s group with the molecular plane as the plane of reflection) correlates adiabatically with $H + CHX(\tilde{a}^3A'')$, and thus the unimolecular decomposition in channel 9 is assumed to be more important between the two.

Based only on energetic considerations, it is difficult to state which of these channels is the main contribution to the slow H-atom feature. However, as the slow component (both the leading edge and the overall shape) shifts to higher E_T in going from CH_3Cl to CH_3Br to CH_3I, its correlation with the dissociation onsets of the three parent molecules can provide some insight into the more likely dissociation channels (assuming the same mechanisms for the three CH_3X based on their similar Rydberg transitions). This shift of slow peak to the higher E_T suggests that extra energy becomes available for the slow channel, which has to involve breaking of the C−X bond of CH_3X or formation of CX product, whose strength decreases in the same order. Based on the thermodynamical values (Table 1), the thresholds of channels 2, 4, and 6 decrease most when going from CH_3Cl to CH_3Br to CH_3I, while that of channel 3 increases, those of channels 5 and 7 decrease slightly [as the decrease in (4) and (6) is compensated by the increasing spin−orbit energy of Cl, Br, to I], and those of channels 8 and 9 stay about the same (due to breaking of the two similar C−H bonds). These trends in the change of the thresholds are indicated by the arrows in Figures 2−4. Channels 2 and 4 [and possibly (5) and (6)] are the more likely candidates for the slow peak, as their thresholds follow the leading edge of the slow peak closely. Channels 3 and 7 are not likely or at least they are not significant for the fast portion of the slow peak, as their thresholds are shifted away from the leading edge for at least one CH_3X. In addition, channels 6 and 7 are not favored in a two-step dissociation mechanism due to symmetry consideration, as discussed before. Channels 8 and 9 (breaking of the second C−H bond) clearly make little contribution to the slow peak, because their thresholds are far away from the leading edge and in addition, in a two-step sequential dissociation mechanism, the population of CH_2X (from the fast peak, channel 1) with internal energy above its dissociation limit is much smaller compared to the slow peak.

In this experiment, the relative branching ratio (by integrated areas) of the fast and slow components decreases from 0.54 to 0.24 to 0.08 in going from CH_3Cl to CH_3Br to CH_3I (Table 2). This trend of increasing relative contribution of the slow peak with the decreasing C−X bond strength could be partially due to an increase in the C−H fission of CH_3 produced after C−X dissociation (channels 4 and 5) or in the triple dissociation channel 2, which is a consequence of increased available energy for the two-step dissociation of the CH_3 fragment and for the triple photodissociation. This observed correlation between the weakness of the C−X bond and the increase of the slow signal could be consistent with channels 2, 4, and 5 being the major contributions of the slow component, as these channels involve cleavage of the C−X bond or production of CX.

4. Dissociation of the Superexcited State of CH_3I. At 121.6 nm, CH_3I is excited to a Rydberg state above the first two ionization limits[13,19] and is in the so-called superexcited state (SES).[31,37,38] It is well-known that when polyatomic molecules are excited into a high Rydberg state within several eV above the first ionization threshold (a SES converging to vibrationally excited ion or higher ionization limit), their ion yields are less than unity, and nonionic decay channels such as neutral dissociation and fluorescence can compete with direct photoionization and autoionization.[31,37,38] As the photoionization fragmentation channel $CH_2I^+ + H$ has an appearance energy of 12.8 eV,[39] this H-atom channel is not open at 121.6 nm. Even if the 365 nm radiation might plausibly contribute to the $CH_2I^+ + H$ channel (e.g., via 121.6 nm photoionization of CH_3I and 365 nm photodissociation of CH_3I^+, with a total photon energy of 13.8 eV), this channel would be open with only ∼1 eV excess energy, which just corresponds to a maximum $E_T \sim 23$ kcal/mol in the $P(E_T)$. In addition, positive ions such as CH_3I^+ formed were removed by the small negative potential below the interaction zone and cannot reach the detector.[22] Therefore, the observed neutral H atoms, particularly the small amount of fast H atoms, should be produced from photodissociation of neutral CH_3I at 121.6 nm. This H-atom signal from CH_3I, similar to those of CH_3Cl and CH_3Br (which dissociate via the similar types of Rydberg transitions but have the first ionization threshold above 121.6 nm photon energy), provides direct evidence that neutral photodissociation of the superexcited CH_3I

molecule competes with direct photoionization and autoionization (into the $^2E_{3/2}$ and $^2E_{1/2}$ state of CH_3I^+).

Acknowledgment. This work is supported by National Science Foundation (CHE-9811400) and, in part, by a UC Regents' Faculty Fellowships and Faculty Development Award, an ACS-PRF Type G Research Grant, and a Camille and Henry Dreyfus New Faculty Award. We thank Prof. Curt Wittig for donating a vacuum chamber used in this work.

References and Notes

(1) Mordaunt, D. H.; Lambert, I. R.; Morley, G. P.; Ashfold, M. N. R.; Dixon, R. N.; Western, C. M.; Schnieder, L.; Welge, K. H. *J. Chem. Phys.* **1993**, *98*, 2054.

(2) Heck, A. J. R.; Zare, R. N.; Chandler, D. W. *J. Chem. Phys.* **1996**, *104*, 3399.

(3) Heck, A. J. R.; Zare, R. N.; Chandler, D. W. *J. Chem. Phys.* **1996**, *104*, 4019.

(4) Brownsword, R. A.; Hillenkamp, M.; Laurent, T.; Vatsa, R. K.; Volpp, H. R.; Wolfrum, J. *Chem. Phys. Lett.* **1997**, *266*, 259.

(5) (a) Evleth, E. M.; Cao, H. Z.; Kassab, E. In *Photophysics and Photochemsitry above 6 eV*; Lahmani, F., Ed. Elsevier: Amsterdam, 1985. (b) Mebel, A. M.; Lin, S. H.; Chang, C. H. *J. Chem. Phys.* **1997**, *106*, 2612.

(6) Wang, J.; Liu, K. *J. Chem. Phys.* **1998**, *109*, 7105.

(7) Jackson, W. M.; Roosevelt, J.; Xu, D.; Wrobel, J.; Ahmed, M.; Peterka, D.; Suits, A. *J. Chem. Phys.* **1995**, *109*, 4703.

(8) (a) Tonokura, K.; Matsumi, Y.; Kawasaki, M. *J. Chem. Phys.* **1991**, *95*, 5065. (b) Tonokura, K.; Mo, Y.; Matsumi, Y.; Kawasaki, M. *J. Phys. Chem.* **1992**, *96*, 6688.

(9) Brownsword, R. A.; Hillenkamp, M.; Laurent, T.; Vatsa, R. K.; Volpp, H. R.; Wolfrum, J. *J. Chem. Phys.* **1997**, *106*, 1359.

(10) Levy, M. R.; Simons, J. P. *J. Chem. Soc., Faraday Trans. 2* **1975**, *71*, 561.

(11) Brownsword, R. A.; Hillenkamp, M.; Laurent, T.; Vatsa, R. K.; Volpp, H. R.; Wolfrum, J. *J. Phys. Chem.* **1997**, *101*, 995.

(12) Lai, L.; Hsu, Y.; Liu, K. *Chem. Phys. Lett.* **1999**, *307*, 385.

(13) Robin, M. B. *Higher Excited States of Polyatomic Molecules*; Academic Press: New York, 1975; Vol. I.

(14) (a) Russell, B. R.; Edwards, L. O.; Raymonda, J. W. *J. Am. Chem. Soc.* **1973**, *95*, 2129. (b) Raymonda, J. W.; Edwards, L. O.; Russell, B. R. *J. Am. Chem. Soc.* **1974**, *96*, 1708.

(15) Truch, D. T.; Salomon, D. R.; Armstrong, D. A. *J. Mol. Spectrosc.* **1979**, *78*, 31.

(16) Szarka, M. G.; Green, D. S.; Cramb, D. T.; Wallace, S. C. *J. Phys. Chem.* **1997**, *101*, 1818.

(17) Hochmann, P.; Templet, P. H.; Wang, H. T.; McGlynn, S. P. *J. Chem. Phys.* **1975**, *62*, 2588.

(18) Causley, G. C.; Russell, B. R. *J. Chem. Phys.* **1975**, *62*, 848.

(19) (a) Wang, H. T.; Felps, W. S.; Findley, G. L.; Rau, A. R. P.; McGlynn, S. P. *J. Chem. Phys.* **1977**, *67*, 3940. (b) Tsai, B. P.; Baer, T. *J. Chem. Phys.* **1974**, *61*, 2047.

(20) Boschi, R. A.; Salahub, D. R. *Mol. Phys.* **1972**, *24*, 289.

(21) Schnieder, L.; Meier, W.; Welge, K. H.; Ashfold, M. N. R.; Western, C. M. *J. Chem. Phys*. **1990**, *92*, 7027.

(22) (a) Xu, K.; Amaral, G.; Zhang, J. *J. Chem. Phys.* **1999**, *111*, 6271. (b) Zhang, J.; Xu, K.; Amaral, G. *Chem. Phys. Lett.* **1999**, *299*, 285.

(23) (a) Zare, R. N. *Mol. Photochem*. **1972**, *4*, 1. (b) Yang, S. C.; Bersohn, R. *J. Chem. Phys*. **1974**, *61*, 4400.

(24) Chase, M. W., Jr. *NIST-JANAF Themochemical Tables*, 4th ed.; *J. Phys. Chem. Ref. Data*, Monograph 9, 1998.

(25) DeMore, W. B.; Sander, S. P.; Golden, D. M.; Hampson, R. F.; Kurylo, M. J.; Howard, C. J.; Ravishankara, A. R.; Kolb, C. E.; Molina, M. J. *Chemical Kinetics and Photochemical Data for Use in Stratospheric Modeling, NASA Evaluation Number 12*; JPL Publication 97-4, 1997.

(26) Lide, D. R. *Handbook of Chemistry and Physics*, 71st ed.; CRC Press Inc.: Boston, MA, 1991.

(27) Kuchitsu, K. *Structure of Free Polyatomic Molecules*; Springer-Verlag: Berlin, 1998.

(28) (a) Schwartz, M.; Marshall, P. *J. Phys. Chem.* **1999**, *103*, 7900. (b) Espinosa-Garcia, J.; Dobe, S. *J. Phys. Chem.* **1999**, *103*, 6387. (c) Poutsma, J. C.; Paulino, J. A.; Squires, R. R. *J. Phys. Chem.* **1997**, *101*, 5327.

(29) Litorja, M.; Ruscic B. *J. Chem. Phys.* **1998**, *108*, 6748.

(30) Murray, K. K.; Leopold, D. G.; Miller, T. M.; Lineberger, W. C. *J. Chem. Phys.* **1988**, *89*, 5442.

(31) (a) Berry, R. S. *Rec. Chem. Prog*. **1970**, *31*, 9. (b) Berry, R. S.; Leach, S. *Adv. Electron. Electron. Phys.* **1980**, *57*, 1.

(32) Freund, R. S. In *Rydberg States of Atoms and Molecules*; Stebbings, R. F., Dunning, F. B., Eds.; Cambridge University Press: Cambridge, UK, 1983.

(33) Even, U.; Levine, R. D.; Bersohn, R. *J. Phys. Chem.* **1994**, *98*, 3472.

(34) Jortner, J.; Bixon, M. *J. Chem. Phys.* **1995**, *102*, 5636.

(35) (a) Kassner, C.; Stuhl, F. *Chem. Phys. Lett.* **1994**, *222*, 425. (b) North, S. W.; Blank, D. A.; Chu, P. M.; Lee, Y. T. *J. Chem. Phys.* **1995**, *102*, 792.

(36) Brownsword, R. A.; Hillenkamp, M.; Laurent, T.; Vatsa, R. K.; Volpp, H. R.; Wolfrum, J. *J. Phys. Chem.* **1997**, *101*, 5222.

(37) Berkowitz, J. *Photoabsorption, Photoionization, and Photoelectron Spectroscopy*; Academic Press: New York, 1979.

(38) (a) Hatano, Y. *Phys. Rep*. **1999**, *313*, 109, and references therein. (b) Nakamura, H. *Annu. Rev. Phys. Chem.* **1997**, *48*, 299. (c) Person, J. C.; Nicole, P. P. *J. Chem. Phys.* **1971**, *55*, 3390. (d) Penner, A.; Amirav, A.; Tasaki, S.; Bersohn, R. *J. Chem. Phys*. **1993**, *99*, 176.

(39) Mallard, W. G., Linstrom, P. J., Eds. *NIST Chemistry WebBook, NIST Standard Reference Database Number 69*; National Institute of Standards and Technology: Gaithersburg, MD 20899, February 2000 (http://webbook.nist.go).